Retracing Schwann cell developmental transitions in embryonic dissociated DRG cultures

Venkat Krishnan Sundaram[1]*, Rasha Barakat[1,2], Charbel Massaad[1], Julien Grenier[1]*

1. Université de Paris, INSERM UMR 1124, Faculty of Basic and Biomedical Sciences, Paris, France.

2. Université de Paris, INSERM UMR 1016, Institut Cochin, Paris, France.

***Correspondance :**

Venkat Krishnan SUNDARAM
venkatkrishnan.sundaram@parisdescartes.fr
https://orcid.org/0000-0001-6024-6959

Julien GRENIER
julien.grenier@parisdescartes.fr
https://orcid.org/0000-0002-1897-1329

Author Contributions:

CM, JG and VKS designed the study. VKS and RB performed the experiments. VKS analyzed the results and wrote the manuscript. CM validated the methodology. JG prepared the figures. All authors reviewed and edited the manuscript. JG and VKS prepared the final draft for submission.

Acknowledgements:

The authors thank Maja Adamsen and Claire Mader from the *Animal House Core Facility* of BioMedTech (INSERM US36/CNRS UMS2009) for the handling of mice used in the study. We also thank the *Cyto2BM Molecular Biology Platform* of BioMedTech Facilities for the research equipment and other services pertaining to the generation of qPCR data.

Funding:

No specific funding was sought for this study. VKS is funded by a PhD fellowship from the French Ministry of Research and Innovation and Université de Paris. RB is funded by a doctoral contract from INSERM U1016, Institut Cochin, Paris.

Conflict of interest:

The authors declare that there is no conflict of interest.

Abstract:

Embryonic Dissociated Dorsal Root Ganglia cultures are often used to investigate the role of novel molecular pathways or drugs in Schwann cell development and myelination. These cultures largely recapitulate the order of cellular and molecular events that occur in Schwann cells of embryonic nerves. However, the timing of Schwann cell developmental transitions, notably the transition from Schwann Cell Precursors to immature Schwann cells, has not been estimated so far in this culture system. In this study, we use RTqPCR to determine the expression profiles of Schwann cell developmental genes during the first week of culture. We first identified stable reference genes that show minimal variation across different experimental time points. Consequently, we normalized the mRNA profiles of Schwann cell developmental genes using the best internal reference genes. We then compared our data to the expression profiles of these genes in developing spinal nerves elaborated in numerous high-throughput and lineage tracing studies. This comparison helped in identifying that Schwann Cell Precursors transition into immature Schwann Cells between the 5th and 7th day *in vitro*. In effect, our data allows for a better understanding and interpretation of DRG culture experiments especially in studies that aim to elucidate the role of a novel gene in Schwann Cell development and myelination.

Keywords: Dissociated DRG cultures, Schwann Cell Precursors, immature Schwann Cells, Development, RTqPCR

Introduction:

Dissociated Dorsal Root Ganglia (DRG) cultures from mouse embryos have long been utilized as a resourceful model for exploring the nuances of Schwann cell development *in vitro* (Taveggia and Bolino, 2018). The co-culture system provides a solid experimental framework to study different aspects of Schwann cell development such as proliferation, migration, differentiation and myelination of neurites (Päiväläinen et al., 2008; Taveggia and Bolino, 2018). Furthermore, it holistically recapitulates the different aspects of Schwann cell development that is observed *in vivo*. Hence, dissociated DRG cultures form an indispensable part of studies that aim to understand the role of a novel gene in Schwann cell development and differentiation.

It is well known that temporal differences exist between Schwann cell development in Dissociated DRG cultures and in developing spinal nerves. In developing spinal nerves of mice, Neural Crest Cells (NCC), destined to a glial fate, differentiate into Schwann Cell Precursors (SCP) and appear in the DRGs at around E11 (Jacob, 2015). Then, SCPs start migrating on nascent axons between E12.5 and E13.5 to populate their peripheral targets. However, at around E15.5 in mice, SCP transition into immature Schwann cells (iSC) that further differentiate into myelinating and non-myelinating Schwann cells perinatally (Monk et al., 2015; Fledrich et al., 2019; Jessen and Mirsky, 2019).

Nevertheless, these observations cannot be used to extrapolate the timing of Schwann cell developmental transitions *in vitro* because of certain technical reasons. Firstly, the DRGs are dissected from mouse embryos towards the end of the 2nd week of gestation (E12.5 or E13.5). At this stage, SCP *in vivo* have started departing from the DRGs and begun migrating on developing axons (Jessen et al., 1994; Jessen and Mirsky, 2005). However, once dissected and dissociated, the DRG cells give rise to sensory neurons and Schwann cell precursors once again *in vitro* (Ratner et al., 2005; Kim and Maurel, 2009; Kim and Kim, 2018). This is rendered possible because of a reservoir of Neural Crest Cells located inside the DRGs that re-differentiate and populate the culture. Therefore, a significant portion of *in vivo* development is repeated in cell culture albeit with a phase difference. Our objective in this study was to better understand these temporal differences in cocultures in an effort to provide a better experimental and inferential framework.

In this research report, we have used RTqPCR to delineate the expression profiles of developmental genes that are expressed in SCP and iSC (*Dhh, Mpz, Cnp, Plp, Mbp, Krox20, Cad19 and Tfap2α*). Their expression pattern was determined in dissociated DRG cultures during the first 7 Days *in vitro* (DIV) at regular intervals of 48 hours. In order to produce robust and reproducible qPCR data, we first sought to identify stable reference genes from 10 candidates (*Actb*, *Gapdh*, *Tbp*, *Sdha*, *Pgk1*, *Ppia*, *Rpl13a*, *Hsp60*, *Mrpl10*, *Rps26*) using a data analysis workflow that we developed recently (Sundaram et al., 2019). This step is crucial as the cell culture environment is dynamic with different cell populations undergoing proliferation and differentiation simultaneously. Hence, arbitrary choice of reference genes without assessing their stability could possibly render biased expression profiles.

We next determined the expression profile of the developmental genes and compared them to their profiles *in vivo.* Previous high-though put studies in Neural Crest Cells and their derivatives in the Peripheral Nervous System have generated extensive data on the differential expression of genes during Schwann Cell development (Buchstaller et al., 2004; D'Antonio et al., 2006). Additionally, we also compared our data to numerous lineage tracing and gene expression studies performed in developing spinal nerves. This analysis helped us in determining the time window where SCP transition into iSC in Dissociated DRG cultures. Indeed, understanding the developmental transitions of Schwann cells in cocultures is crucial for designing rigorous cell culture experiments on Schwann cell development and *in vitro* myelination assays using different Schwann cell mutants.

Materials and methods:

Animals and Tissue Harvesting

Timed pregnant C57Bl6/J mouse at E13.5 was purchased from Janvier Labs. The pregnant mouse was first anesthetized with isoflurane and sacrificed using cervical dislocation. A total of 5 embryos were surgically removed and placed in ice-cold L-15 media. DRGs were harvested from these embryos based on existing protocols (Kim and Kim, 2018; Taveggia and Bolino, 2018). All aspects of animal care and animal experimentation were performed in accordance with the relevant guidelines and regulations of INSERM and Université de Paris (authorization APAFIS#7405-2016092216181520).

Dissociated DRG cultures

A total of 40 DRGs were harvested from each embryo. DRGs were then trypsinized (0.25% Trypsin in HBSS1X) for 30min at 37°C. Trypsinization was stopped using L-15 media containing 10% Horse Serum (Gibco). DRGs were then spun down at 1500 rpm for 5min. The supernatant was removed, and the tissues were resuspended in DRG plating medium (refer to *Media Compositions*). The tissues were then triturated 10-20 times using flamed Pasteur pipettes until a homogenous cell suspension was obtained. Dissociated DRGs were then plated on 12 well plates for each time point –DIV1 (Days *In Vitro* 1*)*, DIV3, DIV5, DIV7. 40 DRGs from each embryo were plated into 8 wells at approximately 5 dissociated DRGs per well. 2 wells were assigned to each time point. The cells were first plated with DRG plating medium for 16h. The following day the medium was replaced by N2/NGF serum free medium to promote neurite growth and Schwann cell proliferation.

Media Compositions

DRG plating media: DMEM with 4.5g/L glucose (Gibco), 10% heat inactivated Horse Serum (Gibco), 1X Glutamax (Gibco), 1X Antibiotic/Antimycotic (Gibco) and 50ng/µL Nerve Growth Factor 2.5S (R&D Systems)

N2/NGF serum free media: DMEM:F12 (Gibco), 1X N2 supplement (Gibco), 1X Glutamax (Gibco), 1X Antibiotic/Antimycotic (Gibco) and 50ng/µL Nerve Growth Factor 2.5S (R&D Systems)

Total RNA isolation

Total RNA was extracted from each sample using 1mL of TRIzol reagent (Ambion Life Technologies 15596018) on ice as described in the manufacturer's instructions with slight modifications. Briefly, 100% Ethanol was substituted for Isopropanol to reduce the precipitation of salts. Also, RNA precipitation was carried out overnight at -20°C in the presence of glycogen. The following day, precipitated RNA was pelleted by centrifugation and washed at least 3 times with 70% Ethanol to eliminate any residual contamination. Tubes were then spin dried in vacuum for 5 minutes and RNA was resuspended in 20µL of RNase resuspension buffer containing 0.1mM EDTA, pH 8. RNA was then stored at -80°C till RTqPCR.

RNA quality, integrity and assay

RNA quantity was assayed using UV spectrophotometry on Nanodrop One (Thermo Scientific). Optical density absorption ratios A260/A280 & A260/A230 of the samples were above 1.8 and 1.5, respectively. The yield (mean ± SD) for each time point is as follows: DIV1 (26.74 ± 2.57 ng/µL), DIV3 (61.3 ± 8.01 ng/µL), DIV5 (51.86 ± 10.8 ng/µL), and DIV7 (77.34 ± 24.04 ng/µL). Furthermore, the extraction protocol used in the study was also validated using Agilent Bioanalyzer (RIN value 9.0 and above).

RTqPCR

500ng of Total RNA was reverse transcribed with Random Primers (Promega C1181) and MMLV Reverse Transcriptase (Sigma M1302) according to prescribed protocols. Quantitative Real time PCR (qPCR) was performed using Absolute SYBR ROX 2X qPCR mix (Thermo AB1162B) as a fluorescent detection dye. All reactions were carried out in a final volume of 7µl in 384 well plates with 300 nM gene specific primers, around 3.5ng of cDNA (at 100% RT efficiency) and 1X SYBR Master Mix in each well. Each reaction was performed in triplicates. All qPCR experiments were performed on BioRad CFX384 with a No-Template-Control (NTC) to check for primer dimers and a No-RT-Control (NRT) to check for any genomic DNA contamination.

Primer design

All primers used in the study were designed using the Primer 3 plus software (https://primer3plus.com/cgi-bin/dev/primer3plus.cgi). Splice variants and the protein coding sequence of the genes were identified using the Ensembl database (www.ensembl.org). Constitutively expressed exons among all splice variants were then identified using the ExonMine database (https://imm.medicina.ulisboa.pt/group/exonmine/ack.html) (Mollet et al., 2010) Primer sequences that generated amplicons spanning two constitutively expressed exons were then designed using the Primer 3 plus software. For detailed information on Primer sequences used in the study, refer to the supplementary table S3.

Amplification efficiencies

The amplification efficiencies of primers were calculated using serial dilution of cDNA molecules. Briefly, cDNA preparations from all the time points were pooled and serially diluted three times by a factor of 10. qPCR was then performed using these dilutions and the results were plotted as a standard curve against the respective concentrations of cDNA. Amplification efficiency (E) was calculated by linear regression of standard curves using the following equation:

$$E=10^{-(1/\text{slope of the standard curve})}$$

Primer pairs that exhibited a theoretical Amplification Efficiency (E) of 1.9 to 2.1 (95% - 105%) and an R^2 value (Determination Coefficient) of 0.98 and above were chosen for this study.

Statistical analysis and Data Visualization

qPCR readouts were analyzed in Precision Melt Analysis Software v1.2. The amplicons were subjected to Melt Curve analysis and were verified for a single dissociation peak at a Melting Temperature (T_m) > 75°C as expected from the primer constructs. The Cq data was exported to Microsoft Excel for further calculations. Each biological sample had 3 technical replicates thereby generating 3 individual Cq values. The arithmetic mean of the triplicates was taken to be the Cq representing the biological sample. The standard deviation (SD) of the triplicates was also calculated and samples that exhibited SD>0.20 were considered inconsistent. In such cases, one outlier Cq was removed to have at least duplicate Cq values for each biological sample and an SD<0.20.

Statistical analyses for reference gene validation were performed according to our qPCR data analysis workflow (Sundaram et al., 2019). Briefly, 10 conventional reference genes were chosen for the study. The Cq values of these genes were first linearized and the Coefficient of variation (CV) for each gene was calculated (Supplementary Table S1). As all the genes exhibited CV < 50%, they were subsequently screened through the NormFinder algorithm in R (https://moma.dk) (Andersen et al., 2004). The algorithm predicted *Tbp* and *Ppia* to be the most stable references. The normalization factor was then determined as the mean Cq value of *Tbp* and *Ppia* for each sample (Supplementary Table S2). Relative expression of target genes was quantified using the $2^{-\Delta\Delta Ct}$ method (Livak and Schmittgen,

2001; Schmittgen and Livak, 2008). DIV1 group was used as the experimental calibrator and data was visualized using Graph Pad Prism v7.0.

To assess statistical difference in relative RNA quantities between groups, One-way ANOVA was performed in Graph Pad Prism v7.0. If statistical significance was observed between the means of the groups, Tukey's post hoc was performed to compare all the 4 groups with each other. The alpha value threshold was set at 5% and the P-values are represented as follows: $P<0.05$ - *, $P<0.01$ - **, $P<0.001$ - ***.

Results:

Progression of dissociated DRG cultures:

We first documented the progression of the culture at Days *in Vitro* (DIV) 1, DIV3, DIV5 and DIV7 using phase-contrast microscopy. At DIV 1, we observed a very sparse population of dissociated cells that comprised of precursors to neurons, Schwann cells and fibroblasts (Figure 1A). At DIV3, however, we could see a neurite network gradually being formed with small bead-shaped cells located on top of neuronal extensions. These cells are presumably migratory Schwann cell precursors (Figure 1B). The neurites then grew out and established a well-connected network by DIV5 (Figure 1C). Schwann cells now densely populated neurites. Flattened Fibroblast like cells were also observed below the Neurite-Schwann cell network. Not much difference was observed between DIV5 and DIV7 except that more connections were established in the neurite-Schwann cell network (Figure 1D). From these observations, we could only deduce that Schwann cell precursors appear between DIV1 and DIV3. The transition of SCP to iSC could not be established, as we did not observe any significant morphological changes in the cells attached to the developing neurites as observed *in vivo* (Jessen and Mirsky, 2019).

Determination of stable reference genes for normalization:

As a prerequisite to determine the expression profiles of Schwann cell developmental genes using RTqPCR, we first identified suitable reference genes for our experimental setting. We chose 10 candidate reference genes and used our data analysis workflow (Sundaram et al., 2019) to determine the two most stable reference genes across all the time points under consideration.

Briefly, we first calculated the Co-efficient of Variation (CV) of the linearized Cq values of reference genes. All reference genes exhibited CV values lesser than 50% (Table 1 and Supplementary Table S1) indicating that they can all be screened by the NormFinder algorithm without compromising its robustness (Sundaram et al., 2019). Consequently, the Normfinder algorithm predicted *Tbp* and *Ppia* as the most stable reference genes with an S value of 0.16 followed by others with higher S values indicating lower stability (Table 1). The algorithm also determines the best combination of two genes for more accurate normalization. In this regard, the algorithm predicted the combination of *Tbp* and *Ppia* as the best with a grouped S value of 0.11 (Table 1).

Expression profiles of Schwann cell developmental genes:

We then determined the expression profiles our target genes using *Tbp* and *Ppia* as internal references (Figure 2). All target genes tested showed considerable variation across the time points when analyzed with one-way ANOVA (Figure 2A – 2H) To determine differences among groups, we performed Tukey's Post Hoc test.

Dhh showed a stark 14-fold increase between DIV1 and DIV3 (Figure 2A). Although the profile seemed to project a downward trajectory after DIV3, the levels of *Dhh* did not vary significantly between DIV3 and DIV7. *Mpz* displayed an initial spike between DIV 1 and DIV3 by about 12 folds, which was similar to *Dhh*. However, the quantity of *Mpz* gradually increased and reached about 17 folds at DIV7.

Cnp expression increased by about 7-folds between DIV1 and DIV3 and maintained a stable profile till DIV7 (Figure 2C). *Plp* showed an initial peak at DIV3 by about 7-folds, which was comparable to that of *Cnp*. However, *Plp* expressed momentarily dropped at DIV5 and reached a plateau by DIV7 (Figure 2D).

Mbp displayed a modest but statistically significant increase by 2-folds between DIV1 and DIV3 (Figure 2E). However, the expression did not increase significantly beyond DIV3. *Krox20* expression did not

vary significantly between DIV1 to DIV5 (Figure 2F). However, at DIV7 we observed a sudden spike by about 4-folds.

Cad19 expression increased almost linearly between DIV1 and DIV5 (Figure 2G). However, between DIV5 and DIV7, we observe a drop in its expression level. *Tfap2α* maintains a flat profile from DIV1 and DIV3 (Figure 2H). It begins to decline after DIV3 and drops significantly to about 0.5 folds at DIV7.

Comparison of *in vitro* and *in vivo* expression profiles:

We then compared the *in vitro* expression profiles with the profiles of the genes assessed from previous gene profiling studies on the Schwann cell lineage (Buchstaller et al., 2004; D'Antonio et al., 2006). We also consulted seminal reviews on Schwann cell developmental markers (Jessen et al., 1994; Jessen and Mirsky, 2005; Woodhoo and Sommer, 2008; Monk et al., 2015) and other gene-specific expression profiling studies to gain a holistic understanding of the literature. A summary of the current consensus on the expression profiles of these genes *in vivo* along with the relevant literature is presented in Figure 3.

The expression of *Dhh, Mpz and Mbp* is upregulated in SCP at around E12.5 in mice (Jessen and Mirsky, 2005; Woodhoo and Sommer, 2008). In DRG cultures, *Dhh*, *Mpz* and *Mbp* expression is increased at DIV3, confirming our observation that SCP appears between DIV1 and DIV3 (Figure 2A and 2B). Interestingly, the profile of *Dhh* after DIV3 shows some minor differences with its expression *in vivo*. In developing nerves, *Dhh* expression is upregulated during the SCP/iSC transition where it reaches a plateau (Parmantier et al., 1999; Buchstaller et al., 2004; Sharghi-Namini et al., 2006). In culture, the expression seemed to decrease progressively as cells progress from DIV3 to DIV7, albeit the differences are not statistically significant (Figure 2A). On the contrary, *Mpz* expression between DIV3 and DIV7 complies perfectly with *in vivo* data (Blanchard et al., 1996; Lee et al., 1997; Buchstaller et al., 2004). *Mpz* expression increases gradually between DIV3 and DIV7 (Figure 2B).

The profile of *Mbp* concurs with its profile *in vivo* with minor differences. In embryonic nerves, *Mbp* expression is detected primarily in SCP at around E12.5 and keeps increasing till E18.5 (Paratore et al., 2002; Buchstaller et al., 2004). In DRG culture at DIV3, *Mbp* expression is increased and reached a plateau at DIV5 (Figure 2E).

Plp is expressed in migrating neural crest cells and Schwann cell Precursors (Timsit et al., 1992; Buchstaller et al., 2004). In developing nerves, *Plp* expression increases in schwann cells between E12.5 and E18.5. (Buchstaller et al., 2004). In DRG cultures, increase in *Plp* expression at DIV3 concurs with *in vivo* data. However, a momentary but significant drop of *Plp* expression is observed between DIV3 and DIV5 but it marginally increases again at DIV7 (Figure 2D).

Data on *Cnp* expression in SCP of embryonic nerves is inconclusive. We analyzed three separate studies that sought to trace *Cnp* expression in the PNS (Gravel et al., 1998; Yuan et al., 2002; Deng et al., 2014). One study demonstrated that *Cnp* is expressed in the satellite cells of DRGs at E14.5 and at the ventral roots at E17.5 but did not comment on its expression in SCPs (Deng et al., 2014). The other two studies dealt with post-natal time points. Nonetheless, our observations suggest that *Cnp* mRNA is expressed in SCP at DIV3 in culture. This observation, however, needs to be verified *in vivo*.

Krox20 is expressed at two different time points during the development of the PNS (Topilko et al., 1994; Voiculescu et al., 2000; Coulpier et al., 2010). At around E10.5, it is first expressed in the boundary cap cells that are located at the dorsal and ventral roots. This is followed by its expression as SCP transition into iSC at around E15.5. It is one of the genes used in the study that can categorically distinguish between SCP and iSC. In our study, Krox20 expression does not change significantly between DIV1 and DIV5. We then see a sudden spike in its expression between DIV5 and DIV7 suggesting that SCP transition to iSC in this time-period (Figure 2F).

To test this hypothesis, we further looked at the expression profile of *Tfap2α*, which is expressed in NCC and SCP but not in iSC (Stewart et al., 2001)(Figure 2H). The downregulation of this transcription factor is indeed required for SCP to transition into iSC in developing nerves (Stewart et al., 2001; Jacob, 2015). Consistent with this observation, *Tfap2α* levels drop by 50% between DIV5 and DIV7 thus providing further evidence of the SCP/iSC transition between DIV5 and DIV7. Moreover, we also assayed the expression levels of *Cad19*, which is the only known gene that is uniquely expressed in SCP but not in NCC or iSC (Jessen and Mirsky, 2005, 2019; Takahashi and Osumi, 2005). *Cad19* expression *in vitro* was the highest around DIV3 and DIV5 but it reduced again at DIV7 reaching to levels comparable to DIV3.

Taken together, these results give a clear picture of Schwann cell developmental transitions *in vitro*. We thus conclude that SCP appear between DIV1 and DIV3. Between DIV3 and DIV5, SCP proliferate and migrate on nascent neurites. At DIV5, SCP begin their transition into iSC and at DIV7 most of the cells present on neurites are iSC.

Discussion:

The objective of this study was to determine the SCP/iSC transition in DRG-SC cocultures using the mRNA expression profiles of Schwann cell developmental genes (*Dhh, Mpz, Cnp, Plp, Mbp, Krox20, Cad19, Tfap2α*). We first identified stable reference genes to normalize the expression of the target genes and determine their profiles. In this study, we have determined *Ppia* and *Tbp* to be the best combination of references genes to normalize qPCR data in dissociated DRG cultures before the induction of myelination. From the normalized profiles of developmental genes, we sought to estimate the time window where SCP transition to iSC in this culture system.

Our data seem to largely comply and concur with the order of molecular events observed in embryonic spinal nerves. However, we pinpoint certain differences in genes such as *Dhh* and *Plp*. We believe that such differences exist due to innate differences between DRG cultures and developing nerves. For instance, SCP which transition into iSC at around E15.5 further differentiate into promyelinating and Remak Schwann cells after radially sorting large caliber axons from smaller ones gradually between E18.5 and P10 (Jessen and Mirsky, 2005; Monk et al., 2015; Fledrich et al., 2019). This is accompanied by an intrinsic change in the expression of Schwann cell developmental genes. *Dhh*, for example, is not expressed in Remak Schwann cells but its expression is maintained in myelinating Schwann cells postnatally (Sharghi-Namini et al., 2006). Similarly, the expression of *Plp* and other myelin related genes such as *Mbp* and *Mpz* is further upregulated in myelinating Schwann cells but not in remak cells (Jessen and Mirsky, 2005; Woodhoo and Sommer, 2008; Salzer, 2015). This is primarily because *Krox20* drives the expression of myelin genes in myelinating cells and its expression in Remak cells in downregulated (Svaren and Meijer, 2008; Woodhoo et al., 2009). Hence, our data on DRG-SC cocultures can only be compared and contrasted to *in vivo* data up until the appearance of iSC in embryonic nerves between E15.5 to E17.5. Further comparison with *in vivo* data can be possible if we assess the expression of these genes using *in vitro* myelination assays. Myelination in coculture can be induced by the addition of Ascorbic Acid (Päiväläinen et al., 2008). Conventionally, ascorbic acid is added at DIV7, which concurs with the molecular profiles of iSC at DIV7 (highest RNA expression of *Krox20*, *Mpz*, *Mbp* and *Plp* coupled with the downregulation of *Tfap2α* and *Cad19*). Thus, deducing the profiles of these genes in myelination assays can further help in comparing *in vitro* and *in vivo* data beyond the SCP/iSC transition.

A notable limitation of our study is that we performed qPCR assays with total RNA extracted from all the cell types in the coculture system. Although most of our target genes are uniquely expressed in the Schwann cell lineage, certain genes such as *Tfap2α* and *Cad19* are not unique to Schwann cells. *Tfap2α* expression has also been documented in sensory neurons (Donaldson et al., 1995; Schmidt et al., 2011). However, in DRG-SC cocultures, the total number of sensory neurons pales in comparison to Schwann cells largely because neuronal cells do not actively proliferate in culture as opposed to SCP or iSC. Hence, it is safe to conclude that the difference we observed in *Tfap2α* expression at DIV7 is largely contributed by SCP transitioning into iSC. This is also supported by the concomitant increase in *Krox20* levels.

Similarly, *Cad19* mRNA is also detected in satellite glial cells (SGC) attached to the neuronal soma (Takahashi and Osumi, 2005). Interestingly, *Cad19* expression is retained in SGC postnatally but it is turned down in SCP as they transition to iSC in nerves (George et al., 2018). In culture, SGC are present attached to neuronal soma. However, their proportion is very minimal when compared to Schwann cells. This is mostly because their proliferation is intrinsically dependent on neuronal size and numbers (Hanani, 2005; George et al., 2018). Hence, although *Cad19* levels drop significantly between DIV5 and DIV7, it remains detectable in sufficient amounts even a DIV7 as its expression in retained in SGC.

Nevertheless, despite these minor limitations, our data provides conclusive evidence that the SCP/iSC transition occurs between DIV5 and DIV7. This information serves as a powerful frame of reference to design, execute and comprehend coculture experiments using WT mice or other Schwann cell mutants.

Figures and Figure Legends

Figure 1

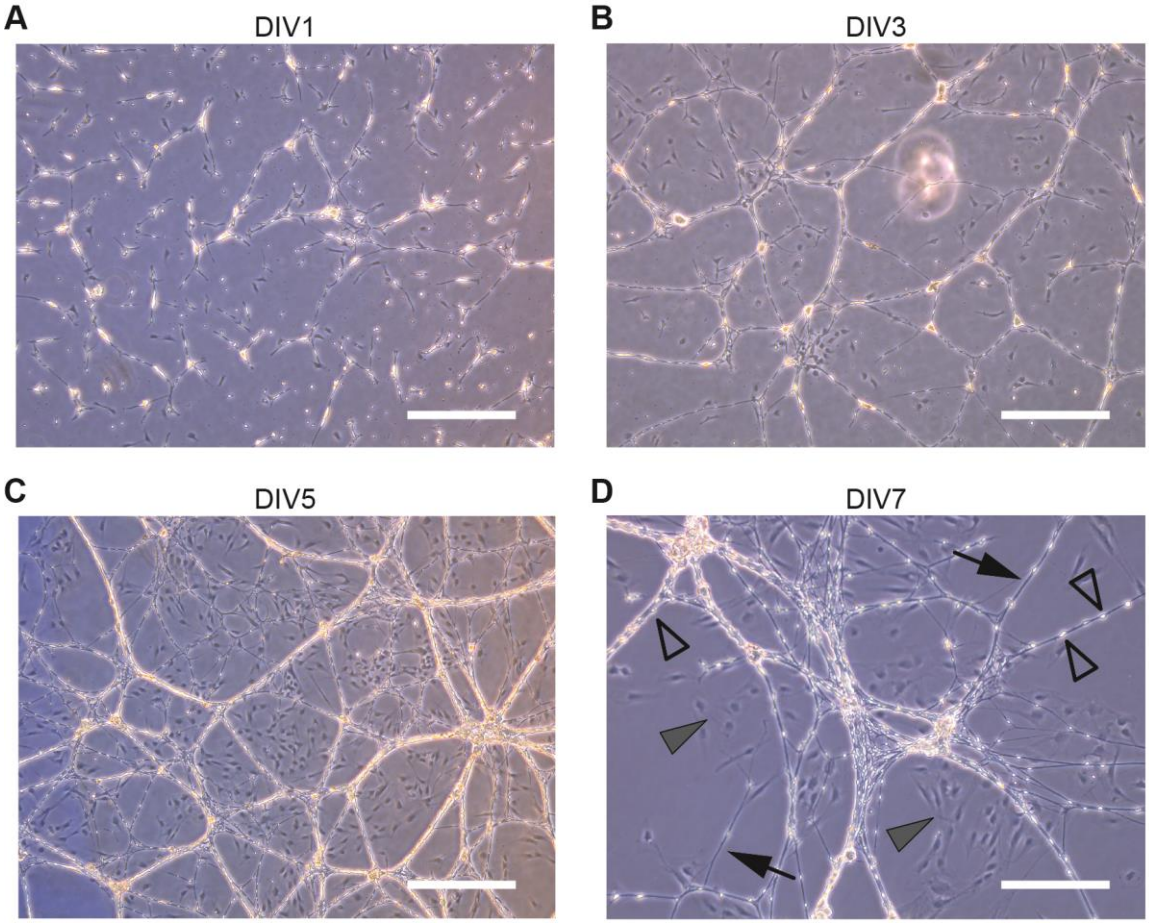

Figure 1: Progression of Dissociated DRG cultures between the first (DIV1) and the seventh (DIV7) day of culture.

Dissociated DRG cells form an extensive network comprised of neurites, Schwann Cells and fibroblasts.

(A) 1 day after plating - DIV1, spindle-shaped neuronal precursors start to form neurite outgrowths. (5X Magnification, Scale Bar = 500µm).
(B) 3 days after plating - DIV3, neurites extend and start to form a mesh like network. Refringent cells attached to the neurites are presumably SCP. Few fibroblasts grow on the bottom of the culture dish beneath the neurite network. (5X Magnification, Scale Bar = 500µm).
(C) 5 days after plating – DIV5, the neurite network is well established and connected. An increase in Schwann cells attached to the neurites is visible when compared to DIV3. Fibroblasts also proliferate in the same time. (5X Magnification, Scale Bar = 500µm).
(D) 7 days after plating – DIV7, the neurite-Schwann cell network now spans the entire dish and all neuronal extensions are covered with Schwann cells. Black arrows indicate neurite extensions. Hollow arrowheads indicate Schwann cells that appear bright under phase contrast. Grey arrowheads indicate flattened fibroblasts that proliferate beneath the network. (10X magnification, Scale Bar = 250µm).

Figure 2

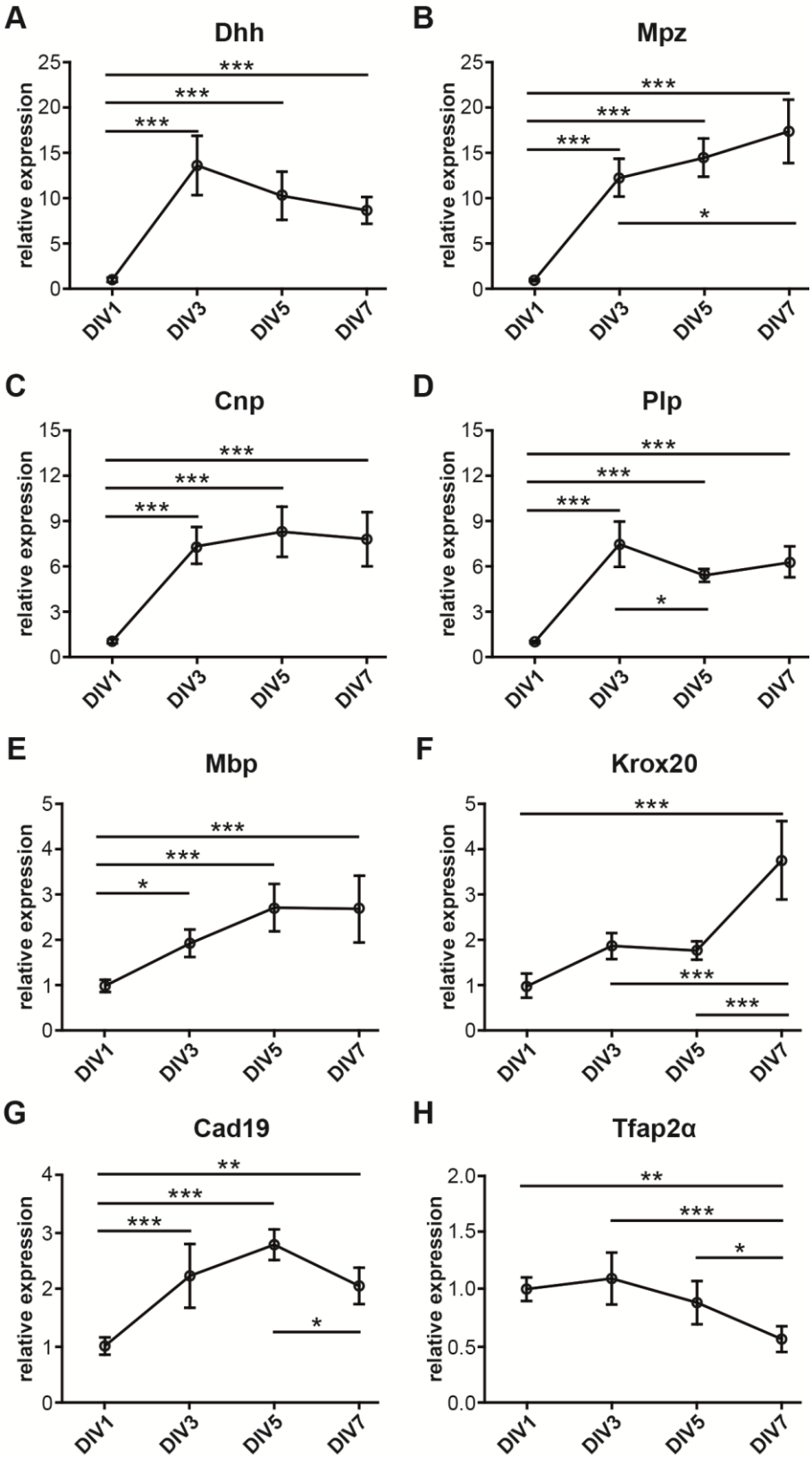

Figure 2: Relative expression of Schwann cell developmental genes during the first week of culture at regular intervals of 48 hours.

Expression profiles of Dhh (A), Mpz (B), Cnp (C), Plp (D), Mbp (E), Krox20 (F), Cad19 (G) and Tfap2α (H) are shown relative to DIV1, which was used as the experimental calibrator. Ppia/Tbp were used as reference genes for normalization. To assess differences across

timepoints, one-way ANOVA was performed followed by Tukey's Post Hoc analysis to compare all the 4 groups with each other. The alpha value threshold was set at 5% and the P-values are represented as follows: * for $P<0.05$, ** for $P<0.01$ and *** for $P<0.001$. Statistically significant comparisons are highlighted with horizontal lines spanning the groups under comparison. Group comparisons that are not highlighted with horizontal lines do not exhibit any statistically significant differences.

Figure 3

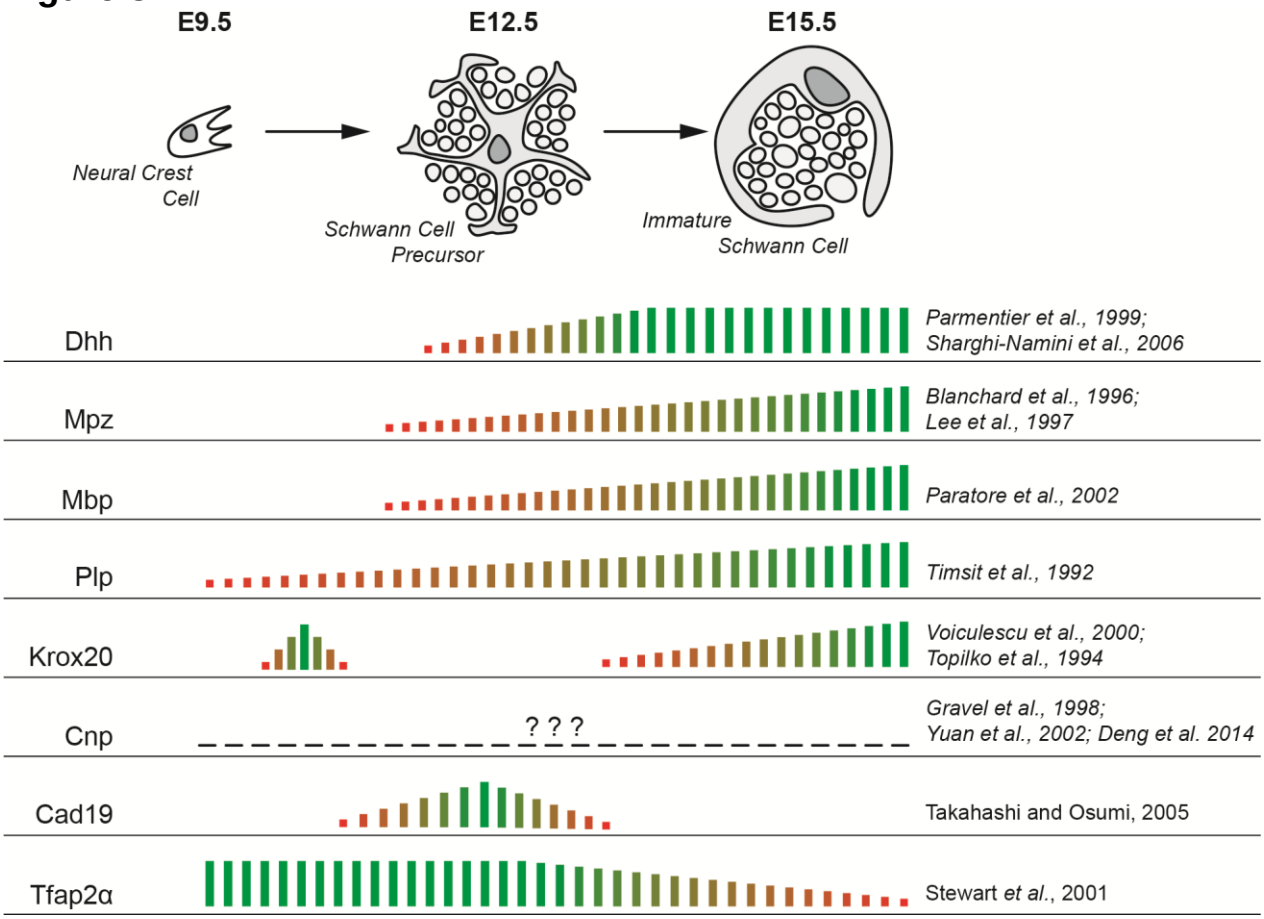

Figure 3: Expression levels of Schwann cell developmental genes in vivo as the transition from SCP to iSC.

The expression levels are expressed as horizontal bars with increasing height indicating higher expression levels. This representation is based on microarray data (Buchstaller et al., 2004) and other high-throughput data (D'Antonio et al., 2006). Additionally, relevant gene profiling and lineage tracing studies are indicated for each gene. Dhh expression begins at the SCP stage and reaches a plateau at the iSC stage. Mpz and Mbp expression is detected at the SCP slightly before the expression of Dhh. Plp is expressed in migrating neural crest cells that are destined towards a glial fate. Krox20 expression occurs in two distinct waves – the first in Boundary Cap Cells that arise from NCC at around E10. The second wave occurs when SCP transition into iSC at E15.5 in embryonic nerves of mice. Cnp expression in the glial lineage is not well documented barring a couple of studies that have documented its expression in satellite glial cells and ventral spinal roots. Cad19 is the only gene know so far that is uniquely expressed in SCP but not in iSC or NCC. Tfap2α is a transcription factor that is expressed from migrating NCC to SCP stages before being downregulated in iSC.

Tables and Table Legends

Table 1

CV analysis	
Gene	**CV%**
SDHA	23.66
MRPL10	23.89
PPIA	25.53
TBP	25.73
GAPDH	29.12
RPL13A	30.94
PGK1	35.13
HSP60	36.29
RPS26	40.15
ACTB	47.27

NormFinder	
Gene	**Stability Value (S)**
PPIA	0.16
TBP	0.16
HSP60	0.22
GAPDH	0.24
RPL13A	0.24
MRPL10	0.34
ACTB	0.37
SDHA	0.38
RPS26	0.39
PGK1	0.44

NormFinder- Best pair of genes	
Gene	**Stability Value (S)**
TBP/PPIA	0.11
HSP60/PPIA	0.14
HSP60/GAPDH	0.15
HSP60/TBP	0.16
GAPDH/TBP	0.18
GAPDH/PPIA	0.18
TBP/RPL13A	0.18
RPL13A/PPIA	0.18
HSP60/RPL13A	0.19
GAPDH/RPL13A	0.22

Table 1: Determination of stable reference genes for qPCR assays on DRG-SC cocultures during the 1st week.

Coefficient of Variation analysis (CV analysis) calculates the overall variation of RNA expression across all samples and time points. It is used to identify genes with high overall variation (CV>50%). Such genes can decrease the performance of the Normfinder algorithm (Sundaram et al., 2019). Normfinder determines the stability of a reference as a weighted measure of its intergroup and intragroup variation (Andersen et al., 2004). The S value calculated by Normfinder ranks the genes from the most to the least stable with the former exhibiting the lowest S value. The method also predicts the best combination of two reference genes that can produce robust qPCR data. In our dataset, Tbp/Ppia combination is found to be the best.

References:

Andersen, C., Jensen, J., and Orntoft, T. (2004). Normalization of Real Time Quantitative Reverse Transcription PCR Data : A Model Based Variance Estimation Approach to Identify Genes Suited for Normalization , Applied to Bladder and Colon Cancer Data Sets. *Cancer Res.* 64, 5245. doi:10.1158/0008.

Blanchard, A. D., Sinanan, A., Parmantier, E., Zwart, R., Broos, L., Meijer, D., et al. (1996). Oct-6 (SCIP/Tst-1) is expressed in Schwann cell precursors, embryonic Schwann cells, and postnatal myelinating Schwann cells: comparison with Oct-1, Krox-20, and Pax-3. *J. Neurosci. Res.* 46, 630–40. doi:10.1002/(SICI)1097-4547(19961201)46:5<630::AID-JNR11>3.0.CO;2-0.

Buchstaller, J., Sommer, L., Bodmer, M., Hoffmann, R., Suter, U., and Mantei, N. (2004). Efficient Isolation and Gene Expression Profiling of Small Numbers of Neural Crest Stem Cells and Developing Schwann Cells. *J. Neurosci.* 24, 2357–2365. doi:10.1523/JNEUROSCI.4083-03.2004.

Coulpier, F., Decker, L., Funalot, B., Vallat, J. M., Garcia-Bragado, F., Charnay, P., et al. (2010). CNS/PNS boundary transgression by central glia in the absence of schwann cells or Krox20/Egr2 function. *J. Neurosci.* 30, 5958–5967. doi:10.1523/JNEUROSCI.0017-10.2010.

D'Antonio, M., Michalovich, D., Paterson, M., Droggiti, A., Woodhoo, A., Mirsky, R., et al. (2006). Gene profiling and bioinformatic analysis of Schwann cell embryonic development and myelination. *Glia* 53, 501–515. doi:10.1002/glia.20309.

Donaldson, L. F., McQueen, D. S., and Seckl, J. R. (1995). Induction of transcription factor AP2 mRNA expression in rat primary afferent neurons during acute inflammation. *Neurosci. Lett.* 196, 181–184. doi:10.1016/0304-3940(95)11870-3.

Fledrich, R., Kungl, T., Nave, K. A., and Stassart, R. M. (2019). Axo-glial interdependence in peripheral nerve development. *Development* 146. doi:10.1242/dev.151704.

George, D., Ahrens, P., and Lambert, S. (2018). Satellite glial cells represent a population of developmentally arrested Schwann cells. *Glia* 66, 1496–1506. doi:10.1002/glia.23320.

Hanani, M. (2005). Satellite glial cells in sensory ganglia: From form to function. *Brain Res. Rev.* 48, 457–476. doi:10.1016/j.brainresrev.2004.09.001.

Jacob, C. (2015). Transcriptional control of neural crest specification into peripheral glia. *Glia* 63, 1883–1896. doi:10.1002/glia.22816.

Jessen, K. R., Brennan, A., Morgan, L., Mirsky, R., Kent, A., Hashimoto, Y., et al. (1994). The Schwann cell precursor and its fate: A study of cell death and differentiation during gliogenesis in rat embryonic nerves. *Neuron* 12, 509–527. doi:10.1016/0896-6273(94)90209-7.

Jessen, K. R., and Mirsky, R. (2005). The origin and development of glial cells in peripheral nerves. *Nat Rev Neurosci* 6, 671–682. doi:nrn1746 [pii]\n10.1038/nrn1746.

Jessen, K. R., and Mirsky, R. (2019). Schwann cell precursors; multipotent glial cells in embryonic nerves. *Front. Mol. Neurosci.* 12, 69. doi:10.3389/fnmol.2019.00069.

Kim, H. A., and Maurel, P. (2009). "Primary Schwann Cell Cultures," in (Humana Press), 253–268. doi:10.1007/978-1-60761-292-6_15.

Kim, J., and Kim, H. A. (2018). "Isolation and expansion of Schwann cells from transgenic mouse models," in *Methods in Molecular Biology* (Humana Press Inc.), 39–48. doi:10.1007/978-1-4939-7649-2_3.

Lee, M. J., Brennan, A., Blanchard, A., Zoidl, G., Dong, Z., Tabernero, A., et al. (1997). P0 is constitutively expressed in the rat neural crest and embryonic nerves and is negatively and positively regulated by axons to generate non- myelin-forming and myelin-forming Schwann cells, respectively. *Mol. Cell. Neurosci.* 8, 336–350. doi:10.1006/mcne.1996.0589.

Livak, K. J., and Schmittgen, T. D. (2001). Analysis of relative gene expression data using real-time quantitative PCR and the 2^-ΔΔCT Method. *Methods* 25, 402–408. doi:10.1006/meth.2001.1262.

Mollet, I. G., Ben-Dov, C., Felício-Silva, D., Grosso, A. R., Eleutério, P., Alves, R., et al. (2010). Unconstrained mining of transcript data reveals increased alternative splicing complexity in the human transcriptome. *Nucleic Acids Res.* 38, 4740–4754. doi:10.1093/nar/gkq197.

Monk, K. R., Feltri, M. L., and Taveggia, C. (2015). New insights on schwann cell development. *Glia* 63, 1376–1393. doi:10.1002/glia.22852.

Päiväläinen, S., Nissinen, M., Honkanen, H., Lahti, O., Kangas, S. M., Peltonen, J., et al. (2008). Myelination in mouse dorsal root ganglion/Schwann cell cocultures. *Mol. Cell. Neurosci.* 37, 568–578. doi:10.1016/j.mcn.2007.12.005.

Paratore, C., Hagedorn, L., Floris, J., Hari, L., Kléber, M., Suter, U., et al. (2002). Cell-intrinsic and cell-extrinsic cues regulating lineage decisions in multipotent neural crest-derived progenitor cells. *Int. J. Dev. Biol.* 46, 193–200. Available at: http://www.ncbi.nlm.nih.gov/pubmed/11902683 [Accessed April 18, 2020].

Parmantier, E., Lynn, B., Lawson, D., Turmaine, M., Namini, S. S., Chakrabarti, L., et al. (1999). Schwann cell-derived Desert hedgehog controls the development of peripheral nerve sheaths. *Neuron* 23, 713–24. Available at: http://www.ncbi.nlm.nih.gov/pubmed/10482238 [Accessed July 18, 2019].

Ratner, N., Williams, J. P., Kordich, J. J., and Kim, H. A. (2005). Schwann Cell Preparation from Single Mouse Embryos: Analyses of Neurofibromin Function in Schwann Cells. *Methods Enzymol.* 407, 22–33. doi:10.1016/S0076-6879(05)07003-5.

Salzer, J. L. (2015). Schwann cell myelination. *Cold Spring Harb. Perspect. Biol.* 7, 1–26. doi:10.1101/cshperspect.a020529.

Schmidt, M., Huber, L., Majdazari, A., Schütz, G., Williams, T., and Rohrer, H. (2011). The transcription factors AP-2β and AP-2α are required for survival of sympathetic progenitors and differentiated sympathetic neurons. *Dev. Biol.* 355, 89–100. doi:10.1016/j.ydbio.2011.04.011.

Schmittgen, T. D., and Livak, K. J. (2008). Analyzing real-time PCR data by the comparative C(T) method. *Nat. Protoc.* 3, 1101–8.

Sharghi-Namini, S., Turmaine, M., Meier, C., Sahni, V., Umehara, F., Jessen, K. R., et al. (2006). The structural and functional integrity of peripheral nerves depends on the glial-derived signal desert hedgehog. *J. Neurosci.* 26, 6364–76. doi:10.1523/JNEUROSCI.0157-06.2006.

Stewart, H. J. S., Brennan, A., Rahman, M., Zoidl, G., Mitchell, P. J., Jessen, K. R., et al. (2001). Developmental regulation and overexpression of the transcription factor AP-2, a potential regulator of the timing of Schwann cell generation. *Eur. J. Neurosci.* 14, 363–372. doi:10.1046/j.0953-816X.2001.01650.x.

Sundaram, V. K., Sampathkumar, N. K., Massaad, C., and Grenier, J. (2019). Optimal use of statistical methods to validate reference gene stability in longitudinal studies. *PLoS One* 14, e0219440. doi:10.1371/journal.pone.0219440.

Svaren, J., and Meijer, D. (2008). The molecular machinery of myelin gene transcription in schwann cells. *Glia* 56, 1541–1551. doi:10.1002/glia.20767.

Takahashi, M., and Osumi, N. (2005). Identification of a novel type II classical cadherin: Rat cadherin19 is expressed in the cranial ganglia and Schwann cell precursors during development. *Dev. Dyn.* 232, 200–208. doi:10.1002/dvdy.20209.

Taveggia, C., and Bolino, A. (2018). “DRG neuron/schwann cells myelinating cocultures,” in *Methods in Molecular Biology* (Humana Press Inc.), 115–129. doi:10.1007/978-1-4939-7862-5_9.

Timsit, S. G., Bally-Cuif, L., Colman, D. R., and Zalc, B. (1992). DM-20 mRNA Is Expressed During the

Embryonic Development of the Nervous System of the Mouse. *J. Neurochem.* 58, 1172–1175. doi:10.1111/j.1471-4159.1992.tb09378.x.

Topilko, P., Schneider-Maunoury, S., Levi, G., Baron-Van Evercooren, A., Chennoufi, A. B. Y., Seitanidou, T., et al. (1994). Krox-20 controls myelination in the peripheral nervous system. *Nature* 371, 796–799. doi:10.1038/371796a0.

Voiculescu, O., Charnay, P., and Schneider-Maunoury, S. (2000). Expression pattern of a Krox-20/Cre knock-in allele in the developing hindbrain, bones, and peripheral nervous system. *genesis* 26, 123–126. doi:10.1002/(SICI)1526-968X(200002)26:2<123::AID-GENE7>3.0.CO;2-O.

Woodhoo, A., Alonso, M. B. D., Droggiti, A., Turmaine, M., D'Antonio, M., Parkinson, D. B., et al. (2009). Notch controls embryonic Schwann cell differentiation, postnatal myelination and adult plasticity. *Nat. Neurosci.* 12, 839–847. doi:10.1038/nn.2323.

Woodhoo, A., and Sommer, L. (2008). Development of the Schwann cell lineage: From the neural crest to the myelinated nerve. *Glia* 56, 1481–1490. doi:10.1002/glia.20723.